Weather and Climate Extremes 38 (2022) 100513

Contents lists available at ScienceDirect

Weather and Climate Extremes

journal homepage: www.elsevier.com/locate/wace

A component-based approximation for trend detection of intense rainfall in the Spanish Mediterranean coast

Juan Javier Miró [a], Marc Lemus-Canovas [b,c], Roberto Serrano-Notivoli [d], Jorge Olcina Cantos [e], Maria.J. Estrela [a], Javier Martin-Vide [c], Pablo Sarricolea [f], Oliver Meseguer-Ruiz [g,*]

[a] Departament de Geografia, Universitat de València, Avda. Blasco Ibáñez, 28, 46010, Valencia, Spain
[b] Andorra Research + Innovation, Rocafort 21-23, AD600, Sant Julià De Lòria, Andorra
[c] Climatology Group, Department of Geography, University of Barcelona, Carrer de Montalegre, 6, 08001, Barcelona, Spain
[d] Departamento de Geografía, Universidad Autónoma de Madrid, Francisco Tomas y Valiente, 1, 28049, Madrid, Spain
[e] Interuniversitary Institute of Geography, University of Alicante, Edificio de Institutos Universitarios, Apartado de Correos, 99, 03080, Alicante, Spain
[f] Departamento de Geografía, Universidad de Chile, CITRID, Programa de Reducción de Riesgos y Desastres, Universidad de Chile, Portugal 84, 8331051, Santiago, Chile
[g] Departamento de Ciencias Históricas y Geográficas, Universidad de Tarapacá, Luis Emilio Recabarren 2477, 1101783, Iquique, Chile

ARTICLE INFO

Keywords:
Iberian peninsula
Non-negative matrix factorization (NNMF)
Synoptic classification
Torrential precipitation
Water-vapor transport

ABSTRACT

Rainfall behavior is a fundamental issue in areas with scarce and irregular amounts, such as the Spanish Mediterranean region. We identified 12 spatial patterns that characterized 899 torrential precipitation events (≥150 mm in 24 h) that occurred in the 3,537 rainy precipitation series in the period 1950–2020. Three of these components—eastern and ESE—showed positive and significant trends in their accumulated volumes. We then characterized the mean synoptic causes of the 10 most intense events in each component at both mean sea-level pressure and 500 hPa geopotential height, and also the integrated water-vapor transport between 1,000 and 300 hPa. We found a clear spatial distribution of the pluviometric effects related to unstable atmospheric situations (such as troughs and cut-off lows), and also to SW–SE advection fluxes that brought moist air from the Western Mediterranean. In particular, torrential rainfall in the Balearic Islands related more to E–NE advections than to southeastern ones. We also determined that the major parts of these components occurred in early autumn, especially in September and October. We expect these findings to help our understanding of the processes leading to catastrophic situations along the Spanish Mediterranean coast and to lead to improvements in early alert systems and management plans.

1. Introduction

Climate change is leading to changes in precipitation in various regions of the world. Precipitation is particularly sensitive to temperature variations and regional changes in atmospheric circulation. Hence, it is difficult to model in climate change scenarios (Miró et al., 2021).

The Mediterranean region is one of the areas of the world where precipitation has a prominent role due to its importance for the development of economic activities that have large territorial and economic imprints (i.e., agriculture and tourism) (Cramer et al., 2018; Ossó et al., 2021; Tapiador et al., 2021), and particularly the Spanish Mediterranean coast (Meseguer-Ruiz et al., 2021). The Intergovernmental Panel on Climate Change (IPCC) AR6 report highlighted the Mediterranean area as a geographical space with a high impact of climate change due to the effect of the warming process on precipitation, pointing out the high probability that more-intense dry sequences will develop, while rainfall episodes will decrease or not change for the southern part of Europe, such as the southern Mediterranean (IPCC et al., 2021).

Several studies on changes in precipitation in the Mediterranean region have analyzed both the impact of warming on regional atmospheric circulation and the effect on precipitation volume and intensity (Cramer et al., 2018; Michaelides et al., 2018).

The change in atmospheric circulation is caused by the existence of a lower thermal gradient between latitudinal bands as a consequence of global warming, which results in a decreased jet stream speed. It has been determined that the average speed of the polar jet stream has decreased by 14% since 1980 (Francis and Vavrus 2012). This implies a greater undulation of the jet—that is, a more-frequent generation of

* Corresponding author.
E-mail address: omeseguer@academicos.uta.cl (O. Meseguer-Ruiz).

https://doi.org/10.1016/j.wace.2022.100513
Received 17 May 2022; Received in revised form 29 August 2022; Accepted 27 September 2022
Available online 28 September 2022

planetary waves with faster displacements of warm air masses towards northern latitudes and of polar or arctic air towards the south. These phenomena are already evident, especially in the Northern Hemisphere, due to the greater effect of warming at polar and subpolar latitudes. This has been linked to the loss of speed of the jet stream (in this case, the polar jet of the Northern Hemisphere), which causes a significant increase in adverse episodes (hot and cold waves, intense drought, and torrential rain) at mid-latitudes, where the Mediterranean area is located (Olcina Cantos et al., 2019).

Muñoz et al. (2020) recently confirmed an increase in cut-off low atmospheric circulation in planetary mid-latitudes, which, in the Northern Hemisphere, has meant an increase of 20% from 1960 to 2017. Moreover, in the European mid-latitude sector, the areas where the installation of these isolated depressions at high atmospheric levels would have been concentrated would correspond to the Gulf of Cadiz, and the Western Mediterranean as a whole (Meseguer-Ruiz et al., 2019; Insua-Costa et al., 2021).

For the specific area of the Spanish Mediterranean coast, Ferreira (2021) analyzed the relationship between intense precipitation and the formation of cut-off lows in the mid-troposphere in the Valencian region between 1998 and 2018, based on the Weather Research and Forecasting (WRF) model. Their results pointed to an increase in heavy precipitation for the next several decades in this region due to an increase in thermodynamic processes in a warmer atmosphere, which is an important nuance to the generally decreasing trend of precipitation over part of the Iberian Peninsula in the last few decades (del Rio et al., 2011).

For the Western Mediterranean Basin, Casanueva et al. (2014) examined changes in the relative contribution of daily rainfall above the 95th percentile to the total amount of rain (R95pTOT) for the period 1950–2010. Using a high-resolution gridded dataset of daily precipitation, they detected that the trend was either significantly positive at specific points or null for most of the areas, but seldom negative. Moliné et al. (2016), based on the EURO–CORDEX model (Representative Concentration Pathways [RCPs] 4.5 and 8.5), studied recent trends in precipitation in the Mediterranean Basin, comparing local and regional scales, and concluding that the extreme rainfall trend could increase by about 10% relative to the current level for RCP4.5 and by around 25% in heavy summer precipitation over some parts of the Iberian Peninsula for RCP8.5. Cipolla et al. (2020) highlighted the role of atmospheric circulation in the occurrence of severe rains in the Sicilian area, especially when the events were characterized by their short duration and high intensity. They also identified the meteorological circulation patterns that were most likely to cause maximum daily precipitation, highlighting the convective component.

Zittis et al. (2021), using a new data-processing procedure on a set of 33 regional climate simulations from the EURO–CORDEX initiative, with a resolution of 0.11°, analyzed the significance of trends for 1951–2000 and 2001–2100 based on the business-*as*-usual RCP—RCP8.5. They reached the conclusion that extreme rainfall events had increased, against a general context of decreasing annual precipitation across the entire Mediterranean Basin.

In Spain, several studies have been carried out on the recent evolution of precipitation, in order to validate the hypothesis of increased daily precipitation in recent decades. In this regard, it has been pointed out that the most-extreme episodes have an increasing probability of occurrence (Myhre et al., 2019) and are linked with the presence of atmospheric rivers (Ramos et al., 2015; Lorente-Plazas et al., 2020; Hénin et al., 2021).

Grimalt-Gelabert et al. (2021) analyzed the synoptic situations that favor the development of extreme torrential rainfall (>200 mm in 24 h) along the Mediterranean coast of the Iberian Peninsula and the Balearic Islands (1941–2010), noting a distinction between trough or cut-off low circulations, which are more favorable for torrential rain episodes in the Balearic Islands, and situations with an eastern component, which cause heavy rains along the Mediterranean coast of the Iberian Peninsula. Senciales-González and Ruiz-Sinoga (2021) examined synoptic types that cause torrential rainfall in the southern Spanish Mediterranean (Andalusian coastal sector), finding than more than 50% of the heavy rainfall events recorded in southern Spain were associated with NE–E and SE–S winds. Specifically, the greatest volumes of precipitation (>100 mm in 24 h) were associated with dynamic low pressure, with front weather types and NE–E winds, although the greatest number of cases occurred with this weather type and SE–S winds.

The role of atmospheric rivers has also been identified for other European latitudes (Lavers et al., 2011; Lavers and Villarini, 2015; Ramos et al., 2018), and they have a tropical origin (Krichak et al., 2015). Aside from this, the role of the Arctic amplification remains insignificant (Blackport and Screen 2020). Insua-Costa et al. (2019) and Davolio et al. (2020) showed that tropical and subtropical moisture inputs are the most relevant for extreme precipitation events in the Western Mediterranean. Cloux et al. (2021) pointed out the need to correctly identify the origin of the humidity in episodes of torrential rain occurring in Southern Europe and especially in the Mediterranean area. They proposed their own model (the offline Lagrangian model FLEXPART–WRF), which allows identification of the local (Western Mediterranean) and medium-distance (Central Mediterranean and North Atlantic) sources that participated in these events.

A report on the future evolution of intense precipitation in Spain (CEDEX 2021), based on the period 1971–2000 and using the EURO–CORDEX climate projections (Horizon 2100), indicated an increase in torrential rainfall, with extreme rainfall associated with short durations for RCP8.5 scenarios, especially over the eastern Iberian Peninsula.

Cardoso et al. (2020) also evaluated future changes in total precipitation in the Iberian Peninsula under the RCP8.5 scenario. The changes were analyzed for two future climate periods—2046–2065 and 2081–2100. They found that, under this climate change scenario, a large part of the region is expected to experience a reduction in annual precipitation of about 20%–40%, reaching 80% in summer, by the end of the 21st century. These results imply that climate change is likely to influence annual precipitation amounts and torrential rainfall events throughout the 21st century, especially in the southern peninsular regions.

Merino et al. (2016) performed a synoptic study of extreme precipitation events occurring between 1960 and 2011, applying a non-hierarchical K-means clustering. They characterized six main synoptic types with which extreme precipitation events would develop, and highlighted that these events in the western peninsular were basically related to zonal circulations, whereas, in the eastern peninsular, they were related to the development of cut-off lows in the mid-troposphere.

Serrano-Notivoli et al. (2018), based on an analysis of the spatial and temporal variability of daily precipitation in Spain for the period 1950–2012, discovered the following significant facts: 1) there was a slight overall increase in the duration of precipitation events, especially along the Mediterranean coast; 2) there was an increase in the frequency of low-precipitation events and a decrease in the frequency of high and very high events (inverse on the Mediterranean coast); and 3) there was a slight decrease in intensity when considering single events (durations of 1 or 5 days), but a significant negative trend in mean and median precipitation when considering all precipitation days, especially on the Mediterranean coast. These results along the Mediterranean coast were related to an increase in convective precipitation, triggered by an increase in potential instability caused by an increase in the Mediterranean Sea surface temperature (Llasat et al., 2021).

Miró et al. (2021) pointed out the trend towards an increase in the frequency of torrential rainfall episodes in the coastal areas of eastern and southeastern Spain, based on the use of Coupled Model Intercomparison Project Phase 5 (CMIP5) global circulation model (GCM) local downscaling in the RCP4.5 and 8.5 emissions scenarios.

Despite the strong relationship existing between the occurrence of torrential precipitation events and synoptic situations, different studies have shown connections to larger-scale patterns (Lopez-Bustins and

Lemus-Canovas 2021; Mastrantonas et al., 2021), which can even lead to seasonal changes (Halifa-Marín et al., 2021; Meseguer-Ruiz et al., 2021). It has been demonstrated that the Western Mediterranean Oscillation index (WeMOi) has a statistically significant influence on the precipitation of the Spanish eastern coast (Lopez-Bustins and Lemus-Canovas 2021; Meseguer-Ruiz et al., 2021). For example, Kim et al. (2019) pointed out that the changes predicted for the summer circulation of the South Asian–Sahara Desert teleconnection will lead to an increase in the meridian circulations of Rossby waves in summer over the basin. It is expected that there will be a predominance of ridges in the central and western parts of the Mediterranean Basin and troughs over the Iberian Peninsula and the Eastern Mediterranean.

The aim of this work is to identify the main torrential events (≥150 mm in 24 h) that have occurred along the Spanish Mediterranean coast between 1950 and 2020, determine their spatial components and trends, and obtain their synoptic characterizations at sea-level pressure (slp) and at 500 hPa (z500), in order to provide new insights into the surface and mid-tropospheric processes associated with torrential precipitation.

2. Methodology and data

2.1. Data series and selection of torrential precipitation events

A total of 3,537 daily precipitation series were used in the study, obtained from two databases standardized to be homogeneous and free of gaps. On one hand, we used the CDRD-HR-EIP database (Miró et al., 2017, 2018), which covers the entire area located between south of Tarragona and north of Almería provinces (Fig. 1). The rest of the analyzed area– including the entire Mediterranean coast of the Iberian Peninsula and the Balearic Islands (Fig. 1) –was covered using the filled series used as the basis for the SPREAD database (Serrano-Notivoli et al., 2017a, b). Most of these daily series (>95%) come from stations of the *Agencia Estatal de Meteorología* (AEMet), supplemented by further data from the *Sistema Integral de Atención al Regante* (SIAR) and the *Fundación Centro de Estudios Ambientales del Mediterráneo* (CEAM). Since these databases only provided data up to 2018, an update was made up to 2020 using new data from all the available AEMet series. In order to fill in possible gaps in these newly observed data, the method developed and used by Miró et al. (2017, 2018) was employed.

The daily 24h accumulations are those recorded between 7am of actual day to 7am the following day. This is according to the way these are recorded in AEMET's network of manual stations, which are the vast majority of those used.

In this way, the final database used covered the entire period of 1950–2020, and all of the analyzed area, plus an additional area at least 100 km inland from the Iberian Peninsula so as to ensure a good spatial interpolation of data at the edges.

From the daily database described above, we isolated those daily events that presented extreme rainfall, exceeding 150 mm in 24 h, at least one or more meteorological stations. Since our interest was focused on obtaining the spatial distribution of components representing affinity between the events, for each of the daily events, we retained not only the data points for ≥150 mm, but also the rest of the precipitation data from all the meteorological stations. Thus, a list of events/dates was compiled that include the daily precipitation for the all stations on those specific days. A total of 899 events were identified between 1950 and 2020.

2.2. Torrential precipitation component selection and trends

We proposed a dimensionality reduction to simplify the rainfall spatial distribution of the 899 events analyzed into a few principal components that would define a good regionalization of the episodes and allow examination of the change in trends of each regional component separately.

However, one problem with the application of the traditional principal component analysis (PCA) technique is that daily rainfall forms a non-negative data matrix, in that it does not behave like an oscillator on a central mean, but rather as isolated peaks above zero. Daily torrential events also have a very high dispersion and sparsity. Thus, when applying PCA, we obtained unsatisfactory results that did not allow a

Fig. 1. Administrative division and physical characterization of the study area.

good regionalization.

Several dimensionality reduction techniques are currently available. After an exploratory exercise, we found a technique– the non-negative matrix factorization (NNMF) method (Sra and Dhillon 2006; Tandon and Sra 2010) –that was much better adapted to this type of data, resulting in a much better regionalization and clear geographic linkage of the components obtained. It is a technique especially adapted to dealing with inherently non-negative data, including in the context of high sparsity, with the ability to reduce such sparsity to simpler and more robust components that reflect the most relevant characteristics of the information without overfitting (Tandon and Sra 2010). Therefore, it was a particularly suitable technique for this case.

The NNMF toolbox for MATLAB (https://github.com/jkschluesener/nmf_toolbox_matlab) was used to obtain the components, based on the algorithm developed by Li and Ngom (2013). The option used for the distance in the objective function was the Kullback–Leibler divergence.

As with PCA, NNMF provides, on one hand, a matrix of basic components obtained after reduction of the dimensionality—spatial in this case—so that we could analyze trends of change in each component over time. On the other hand, it allowed us to calculate the weight or contribution of each component to variability in the time-series at all stations, or to reconstruct these series as a sum of weights. Thus, each component would be reconstructed separately, in order to capture its spatial behavior on a map (Fig. 2). In addition, this allowed us to associate each event with the component that predominated, having the greatest weight on the day of the event. We then classified each of these events under each component identified. That is, the component that registers a greater weight in the event is the factor that classifies the event within the concrete type associated that component.

By taking the list of dates/events associated with each component, we could test the hypothesis that each rainfall component obtained would be associated with a predominant synoptic configuration on those dates. We could also relate a change trend obtained for a component with changes in the frequency or strength of that synoptic type.

To obtain the trends of change, the slope was calculated using the nonparametric Sen method (Sen, 1968), which is more robust to outliers than obtaining the simple linear trend. This is important given that extreme precipitation presents high temporal irregularity and very pronounced peaks, which makes it difficult to discern reliable trends from random results. The slope is expressed in mm per decade. Also, in order to test statistically significant change trends for each component, we applied the non-parametric Mann–Kendall test (Mann 1945; Kendall

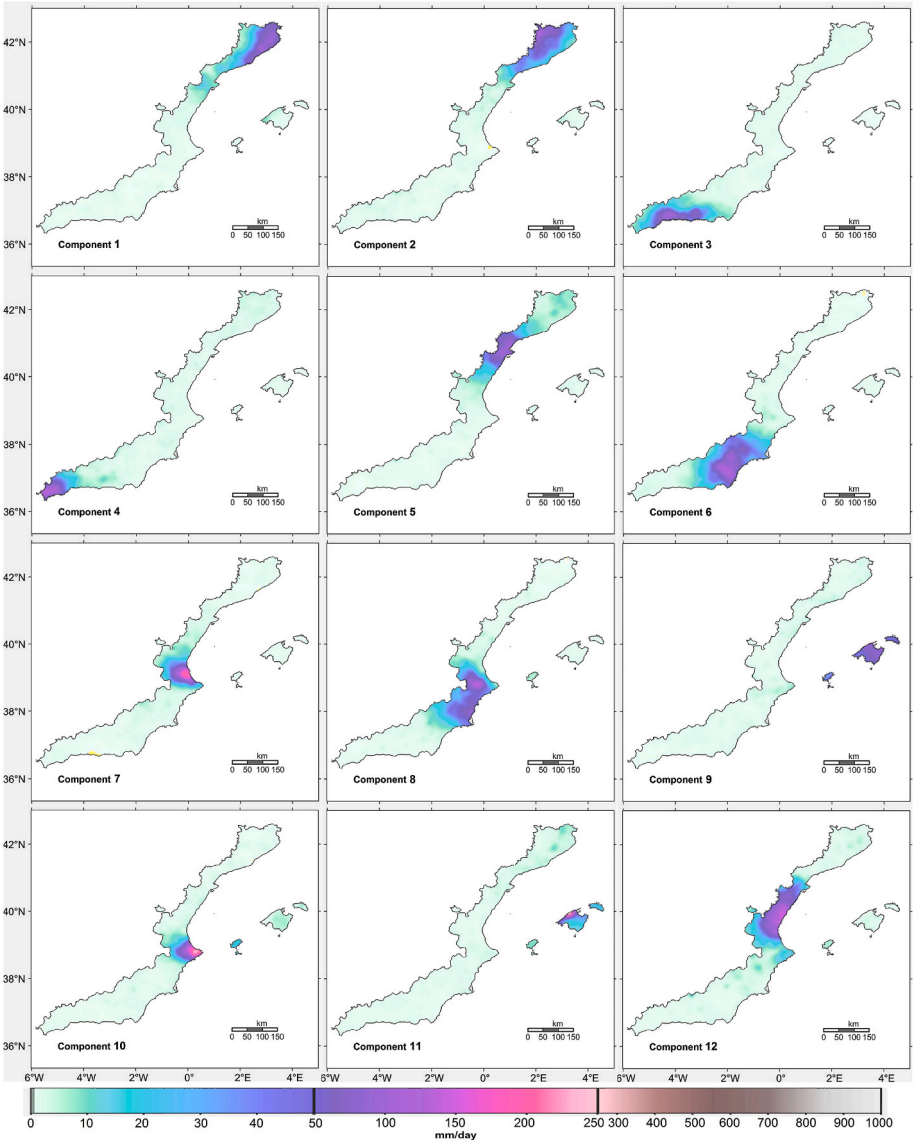

Fig. 2. Spatial components for the identified extreme precipitation events. The spatial distribution represents the mean distribution of values (mm/day) above the 95th percentile for each component.

1962).

These trend-tests were initially applied for the annualized mean precipitation registered for each component (average annual weight). The obtained trends were considered to be statistically significant when satisfied that $\alpha \leq 0.05$ (p-value), giving a confidence level greater than 95%.

The average annual volume obtained for each component was generally low (between 4 and 7 mm) (Table 1) because, although there were local peaks of ≥150 mm per event, the average weight obtained from the entire analyzed territory was obviously much lower. This allowed us to test the overall trends presented by the events associated with a specific component in a more reliable way, and linked to a spatial distribution, but this may not be entirely representative of the extreme precipitation that actually occurred in the specific locations where 150 mm was exceeded.

Table 1
Trends (slope per decade) and changes for whole period analyzed for the different components in the study period (1950–2020) according to the annual volumes (average of entire spatial distribution, and percentiles 95th and 99.9th). Significant trends (confidence level >95% for sen slope and p-value < 0.05 for Mann-Kendall test) are written in bold.

Average annual weight over the average of the whole territory analyzed (mm)				
Component	Average all stations (mm)	Sen slope (mm/decade)	Absolute change for whole period 1950–2020 (mm)	Relative change for whole period 1950–2020 (%)
1	5.65	−0.18	−1.23	−19.7
2	6.26	−0.15	−1.04	−15.4
3	3.93	0.09	0.61	16.9
4	5.50	0.19	1.34	27.8
5	5.42	−0.08	−0.57	−9.9
6	**5.59**	**0.34**	**2.44**	**55.9**
7	**5.49**	**0.33**	**2.32**	**53.4**
8	**6.55**	**0.50**	**3.58**	**75.3**
9	5.61	0.19	1.36	27.6
10	4.27	0.34	2.42	78.9
11	6.42	0.06	0.43	6.9
12	6.92	0.03	0.23	3.3
95th percentile for entire spatial distribution (all stations) of annual precipitation (mm) for each component				
Component	95th prctile value in mm (annual basis)	Sen slope (mm/decade)	Absolute change for whole period 1950–2020 (mm)	Relative change for whole period 1950–2020 (%)
1	31.67	−0.64	−4.52	−13.32
2	38.66	−1.87	−13.25	−29.26
3	17.42	−0.31	−2.18	−11.80
4	48.39	2.30	16.33	40.60
5	25.64	−0.41	−2.88	−10.65
6	29.95	0.87	6.15	22.89
7	31.72	0.41	2.92	9.64
8	**35.53**	**3.37**	**23.91**	**101.41**
9	31.74	0.46	3.28	10.91
10	25.90	1.25	8.88	41.35
11	40.74	0.80	5.68	14.99
12	49.16	−0.14	−0.99	−1.99
99.9th percentile for entire spatial distribution (all stations) of annual precipitation (mm) for each component				
Component	99.9th prctile value in mm (annual basis)	Sen slope (mm/decade)	Absolute change for whole period 1950–2020 (mm)	Relative change for whole period 1950–2020 (%)
1	116.96	−1.09	−7.73	−6.40
2	140.54	−6.29	−44.64	−27.41
3	68.04	−0.31	−2.22	−3.21
4	200.29	15.85	112.56	78.16
5	87.85	−2.17	−15.43	−16.15
6	108.21	1.88	13.36	13.16
7	124.06	2.74	19.44	17.00
8	**115.43**	**12.29**	**87.28**	**121.59**
9	129.89	4.15	29.50	25.62
10	121.87	5.39	38.29	37.27
11	210.89	5.64	40.06	20.99
12	165.84	2.58	18.30	11.68

In order to obtain a more realistic analysis of the precipitation extremes themselves, trends have also been calculated for the 95th and 99.9th percentile value of the annualized data of the components. In this case they have been calculated on the total spatial distribution of their values on an annual basis. That is, the 95th and 99.5th percentile of 3,537 values obtained (stations) for each year and then obtain their trend over the 71 years analyzed.

In any case, if we were only to consider the specific absolute limit of ≥150 mm, we would have some difficulties when only considering the daily accumulated values, and representing the averages of those per station, because the greater the entire rainfall volume, the greater the number of stations recording ≥150 mm, which in turn would lower and misrepresent the average volume per station that reached this threshold. In the same way, several events can be concentrated in one year, so there will not be a maximum, but several, per station. Then, to obtain an idea of whether the truly precipitation ≥150 mmm of each component behaved evenly with the trend of the entire component, we did the following. We considered the total annual volume of recorded precipitation that was actually ≥150 mm and assigned to an event type and divided that volume by the average annual number of stations for the entire 71-year period that actually recorded ≥150 mm for each event and component, instead of by the number of stations that recorded ≥150 mm in that year. The accumulated rainfall was representative of torrential precipitation that reached ≥150 mm, without the effect of variability in the number of observatories reaching 150 mm as a divisor. The results are presented in Fig. 3, and are compared with the trends and their statistical significance in Table 1.

It is important to note that, unlike in PCA, the number of components obtained by NNMF is not fixed and defined by the process itself, but is an adaptive function to a desired number of components, depending on whether greater simplicity or explanatory complexity is sought. Although this may be an advantage, it also brings the disadvantage of having to discern which number of components best explains a regionalization based on the geographical constraints of the area without falling either into oversimplification or having redundant components. This is a case in which user knowledge of the territory may play an important role.

In this sense, the study area was divided into two peninsular areas, clearly defined in terms of their general orientation towards the Mediterranean Basin—one eastern, looking east (territories belonging to Catalonia, Valencia, Murcia and eastern Almeria), the other southern, looking south (belonging to Andalusia), plus an insular area (Balearic Islands). The eastern area represented a relatively wide range of latitudes, this being the factor that allowed us to distinguish several different sectors (e.g., north-central Catalonia, south of Catalonia/Bajo Ebro). The southern area represented a certain range of longitudes, this being the discriminating factor along the southern Mediterranean strip. In both areas, some inland areas could be distinguished by their continentality.

To the discriminating effect of the above geographical factors, we added: 1) the importance of the southern Gulf of Valencia—the area with the highest daily precipitation in Spain and one of the most outstanding in Europe, making it expedient to consider more than one pattern; 2) the southeastern peninsular, as it is one of the driest areas in Europe, where the two peninsular areas considered were also located; and 3) the sector near the Strait of Gibraltar—a pathway for the penetration of Atlantic depressions and flows. In the case of the insular area—the Balearic Islands—the consideration of two sectors was due to the energetic orography of the island of Mallorca, which was singled out as a northwestern sector.

Considering all these criteria, we computed the NNMFs for five to 18 components, ultimately deciding to work with 14 components and then deleting two because they showed an interior component, making 12

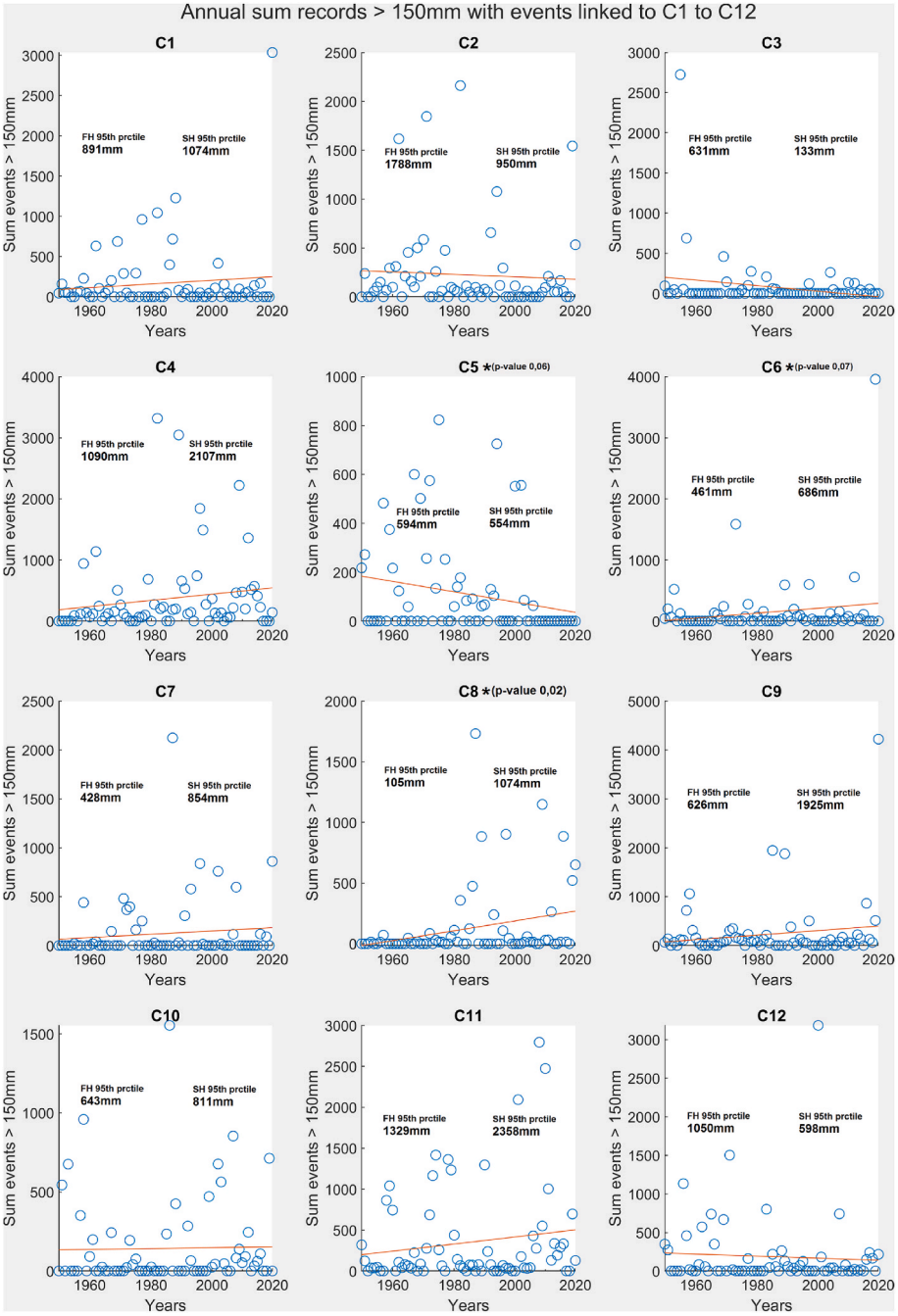

Fig. 3. Annual accumulated records ≥150 mm in 24 h and trends of each component in the study period (1950–2020). For a single event ≥150 mm were exceeded at any one weather station, all amounts recorded in that same event have been considered. Asterisk indicates that the slope is significant (or near significant). 95th percentile of distribution is showed for: FH = first half of period (1950–1984) and SH = second half of period (1985–2020).

components, which was the same number used by Gil-Guirado et al. (2022).

2.3. Synoptic characterization of torrential precipitation events

We used mean slp and a geopotential height of 500 hPa (z500) to compute the average components of the most representative days for each component of the classification. These gridded variables were supplied by the fifth European Centre for Medium-range Weather Forecasts Re-analysis (ERA-5) (Hersbach et al., 2020) by means of daily mean values, encompassing the area 25°N–70°N and 30°W–30°E at a horizontal resolution of 0.25° for the period 1950–2020. To complement the explanation of the synoptic mechanisms that led to such extreme events, we computed the vertically integrated water-vapor transport (IVT) between the 1,000 and 300 hPa levels, following the methodology proposed by Lavers et al. (2012):

$$IVT = \sqrt{\left(\frac{1}{g}\int_{1{,}000hPa}^{300hPa} q \bullet u \bullet dp\right)^2 + \left(\frac{1}{g}\int_{1{,}000hPa}^{300hPa} q \bullet v \bullet dp\right)^2} \quad (1)$$

where q is the specific humidity (kg•kg^{-1}); u and v are the layer-averaged zonal and meridional winds (m•s^{-1}), respectively; g is the acceleration due to gravity (9.8 m•s^{-2}); and p is the pressure difference between two adjacent pressure levels (Pa).

3. Results

3.1. Torrential precipitation events

We identified 12 spatial components for torrential precipitation events in the study area (Fig. 2), with a northern sector (Components 1 and 2) with maximum daily precipitation amounts of between 150 and 200 mm in 24 h, a central sector (Components 5, 7–12) with maximum daily precipitation amounts that reached 300 mm in 24 h, and a southern sector (Components 3, 4 and 6) with maximum daily precipitation amounts of around 150 mm in 24 h.

Components 1 and 2 appeared in the north of the study area, in the Girona and Barcelona provinces. Component 1 exhibited a coastal distribution, with maximum daily precipitation amounts of between 150 and 200 mm in 24 h, while Component 2 showed an inland distribution, with peaks of around 150 mm in 24 h. Component 3 occurred in the south, centered in the coastal area of the Málaga and Granada provinces, and reaching maximum daily precipitation amounts of around 150 and 200 mm in 24 h. Component 4 also showed a southern distribution, constrained to the Málaga province, with maximum daily precipitation amounts of precipitation of around 180 mm in 24 h. Component 5 events were centered on the Ebro River delta, extending from 40°N to 42°N, with precipitation daily precipitation amounts also reaching 180 mm in 24 h. Component 6 was located in the southeast, between the provinces of Almería and Murcia, and exhibited maximum daily precipitation amounts of 170 mm in 24 h. Component 7 had its maximum located in southern Valencia province, and reached maximum daily precipitation amounts greater than 200 mm in 24 h. Component 8 was mainly located in the province of Alicante, but also affected southern Valencia, reaching daily precipitation amounts of around 150 mm in 24 h. Component 9 was distributed across all the Balearic Islands, and also reached daily precipitation amounts of 150 mm in 24 h. Component 10 was located in the coastal areas of southern Valencia and northern Alicante (Cabo de la Nao area), and reached daily precipitation amounts of 300 mm in 24 h. This also affected the western Balearic Islands. Component 11 also appeared in the Balearic Islands, but its maximum daily precipitation amounts was centered on the north of the island of Mallorca, reaching 300 mm in 24 h. Component 12 spread from northern Valencia province to southern Tarragona province, and reached daily precipitation amounts of around 150 mm in 24 h.

In terms of trends in the annual amounts of precipitation registered by each component, only three components exhibited significant trends during the study period (Table 1), and these all had positive trends and corresponded to the eastern and southeastern areas. Component 6, with an average of 5.59 mm in each pixel, increased by 2.44 mm (55.9%), Component 7, with a 5.49-mm average, increased by 2.32 mm (53.4%), and Component 8, with an average of 6.55 mm, increased by 3.58 mm (75.3%) between 1950 and 2020. Component 9 and 10 with also notable increases are close to being significant as p-value yet <0.1. For extreme values (Table 1 – 95th and 99.9th percentiles) only Component 8 maintains a positive trend that is statistically significant (Component 5 is close to being significant as p-value yet <0.1), probably due to greater irregularity towards the extremes. But it is important to note that the percentage increases are more pronounced as more extreme percentiles are analyzed. Thus, more than 100% increase in the case of the value represented by the 99.9th percentile for Component 8.

Fig. 3 shows the summed volumes per year per component associated only with those rainfall records that actually recorded $\geq$150 mm at specific stations, divided by the average number of stations that, in a normal year, recorded $\geq$150 mm (as explained in Section 2.2). Note that, in Fig. 3, we identified years with an annual volume that was $<$150 mm, meaning not only a lower volume, but also that there was a smaller number of stations recording $\geq$150-mm events than normal, where the volume was divided by a higher number (i.e., an average of the 71 years). Similarly, there were records that reached 4,000 mm, meaning events where, apart from higher point volumes with $\geq$150 mm, a very large number of stations (higher than the normal divisor) exceeded 150 mm, thereby contributing a larger sum to the total volume. Therefore, this reflected torrential events in a context of equal conditions for interannual comparison throughout the series. In this case, the three components that showed statistically significant positive trends (Table 1) coincided with a positive slope in the trend line for these components in Fig. 3. This was especially intense for Component 8, focused on the area between the eastern Murcia, Alicante, and southern Valencia provinces.

3.2. Weather types

Below are the descriptions of the 12 basic synoptic weather types that caused intense precipitation along the Spanish Mediterranean coast, as established in this study (Figs. 4–6).

1) Low pressure over the Balearic Sea, with eastern advection in Catalonia and a high transport of water vapor in this area, causing large amounts of precipitation in the coastal mountain systems perpendicular to the eastern flow. The southern part of the study area was not affected because it was located just beneath the cold core of the low, where there was less rainfall activity. This situation showed an absolute peak of relative frequency in April.
2) A northwestern trough with low pressure, located along the coasts of Portugal and Galicia, promoting a southwestern flow towards the north of the study area. This type of flow was very productive in the north of the study area, especially in the pre-Pyrenees and the Catalan coastal ranges. These surface conditions, together with a high amount of water-vapor transport, favored high accumulated precipitation in this area. This pattern was characteristic of September and October.
3) The position of the W–SW low favored S–SE advection in the southern half of the study area, bringing a significant amount of water vapor of Atlantic origin from subtropical latitudes to the extreme south (Malaga and Granada). This type of circulation was particularly prevalent at the beginning and end of the cold half of the year (from October to March).
4) The location of a low-pressure cell in the northwest is a typical winter situation resulting from a southward displacement of the extratropical jet, which favors the circulation of cyclones at latitudes below 45°N and allows southwestern advection. This type of advection was very productive in the southwest of the study area, since it presented an orthogonal orientation to the mountain ranges of the province of Malaga, favoring a certain orographic component as a triggering mechanism for high amounts of precipitation.
5) A cut-off low in the northwest, with weak surface flow from the east with an upper level of cold air, but without a marked baric gradient at the surface. This also showed a weak easterly flow directly affecting the area between the provinces of Castellon and Tarragona, perpendicular to the disposition of the eastern end of the Iberian Mountain range. In fact, this situation was not marked by a high contribution of water vapor, with the rainfall amounts being closely associated with orographic precipitation. This type had a peak frequency in October.
6) An eastern flow with a cut-off low in its upper level occurring to the southwest. The situation of the upper-level trough was most active in its easternmost part, favoring instability in the southeast of the study area (Granada, Almería, and Murcia). The easterly flow accentuated the maritime and moisture contribution—a fact that was also noted in the IVT composite. This was a characteristic situation occurring in September.
7) Eastern advection with an upper-level cut-off low. The location of the cut-off low, in this case, was more to the north and east than in the previous case and, together with the easterly flow, contributed to large amounts of precipitation in the province of

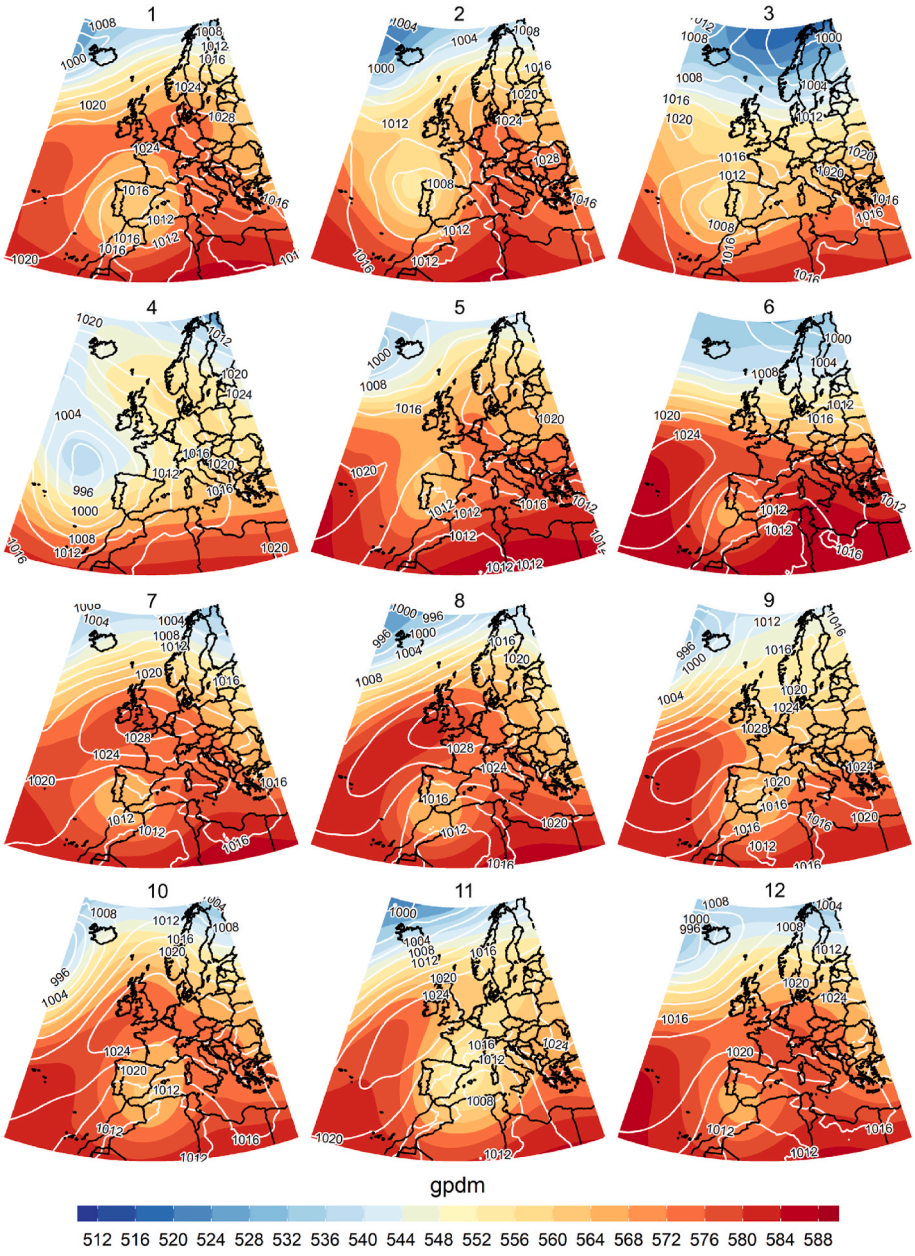

Fig. 4. Sea level pressure (slp; isolines, hPa) and 500 hPa geopotential height (z500; shaded colors, dm) composite of the top ten most intense episodes for each component (1950–2020). (For interpretation of the references to color in this figure legend, the reader is referred to the Web version of this article.)

Valencia, with a more northerly location than those mentioned in the previous pattern. Again, this was a situation characteristic of the autumn months (September–November), although it also occurred in spring. The water vapor had a subtropical origin, transported from North Africa.

8) Eastern advection with an upper-level cut-off low (very similar to Type 7). An upper-level low pressure appeared slightly more to the south than in Type 7, producing high amounts of precipitation, mainly in the provinces of Alicante and southern Valencia, due to the presence of the Betic ranges, which also triggered orographic rainfall. Types 7 and 8 are very similar. They were distinguished by the territorial distribution of the rain they caused, rather than by their synoptic differences.
9) An upper-level cut-off low with surface flow from the east. This was the second most easterly location of the upper-level cut-off, together with Type 11, in both cases causing torrential rainfall in the Balearic Islands. It also had an E–NE surface advection, which triggered higher accumulations in Mallorca and Menorca.
10) A rhombic configuration with an upper-level cut-off low and E–NE surface flow. This was a situation where water-vapor transport was important, impacting the northern edge of Alicante and the southern edge of Valencia. This, together with the E–NE surface flow, favored torrential rainfall in this area and, to a lesser extent, in Ibiza. Its maximum frequency was in April, but it also had a marked presence throughout the autumn.
11) A trough in the Western Mediterranean, with low pressure at both the surface and upper levels, located between the Balearic Islands and Corsica and Sardinia. This type occurred more frequently in the fall. The surface flow was NE–N, with no excessive water-vapor transport. In fact, this type had a high orographic component, since the maximum accumulated in the northern part of the island of Mallorca, where the Tramuntana mountain range (1,400 m a.s.l.) is located.

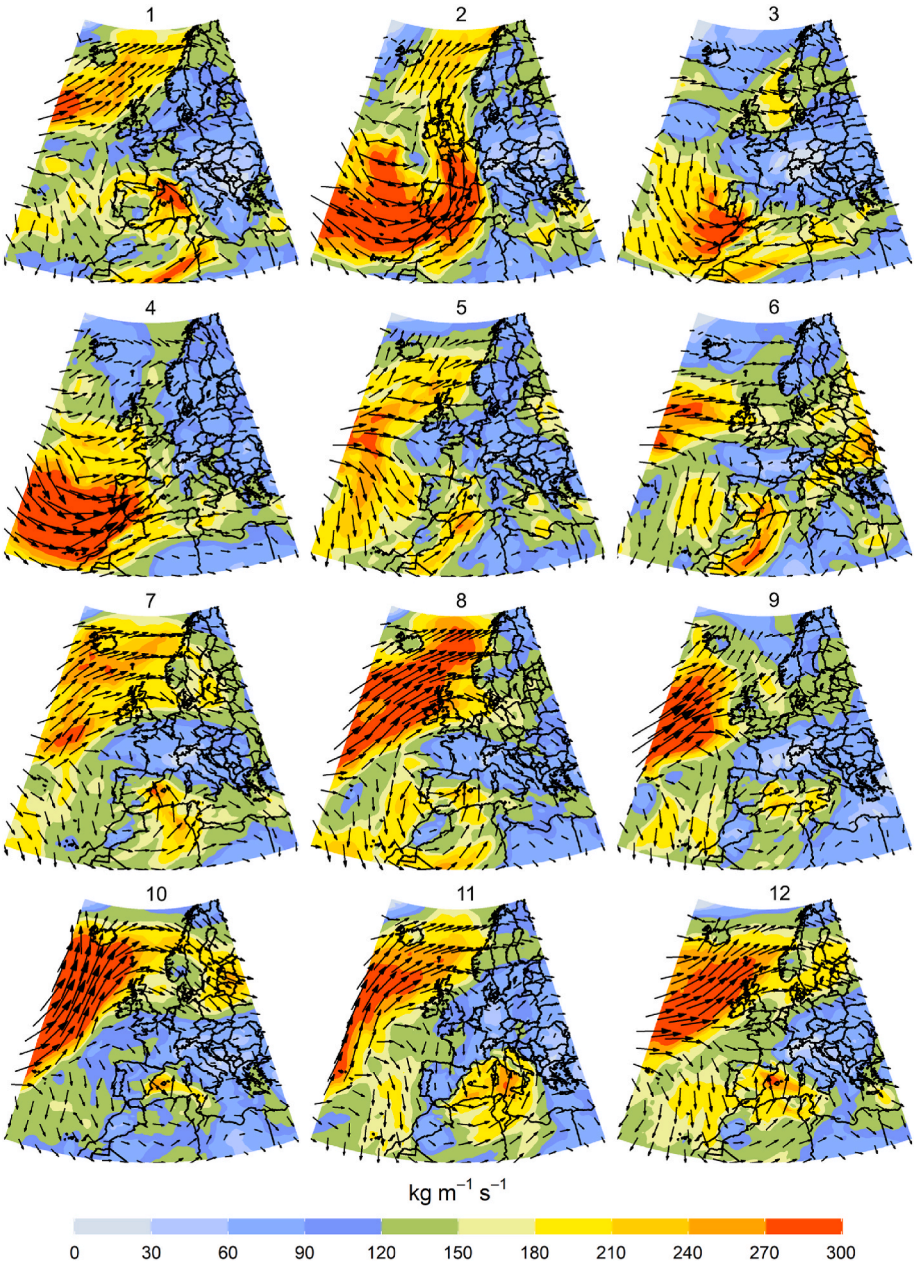

Fig. 5. Vertically integrated water vapor transport (IVT) intensity (shaded colors, kg m−1 s−1) and direction (vectors) composites of the top ten most intense episodes for each component (1950–2020). (For interpretation of the references to color in this figure legend, the reader is referred to the Web version of this article.)

12) An upper-level cut-off low with a weak E–SE surface flow. This appeared exclusively in the fall, with large rainfall accumulations occurring in the provinces of Castellon, northern Valencia, and extreme southern Tarragona. The transport of water vapor was deeply associated with the maximum accumulated rainfall in the area.

There was a strong relationship between the areas of maximum precipitation and the installation of sectors of strong instability in higher layers (500 hPa) with strong vorticity advection. There was also coincidence with an entry of atmospheric humidity into lower layers that dragged the winds of the maritime component. On the northern Mediterranean coast (Catalonia), the highest daily precipitation values corresponded to troughs and cut-off lows, their cores located over the center of the Iberian Peninsula or over Portugal (Components 1, 2, and 5). When this trough (or cut-off low) descended to latitudes below 35°N, the most affected area was the Andalusian Mediterranean coast (Components 3 and 4). The central area (Valencia, Murcia, and the Balearic Islands) was affected by a greater number of components (Components 6–12) that involved the installation of areas of strong positive vorticity in the Strait of Gibraltar or the Alborán Sea. In general, if the axis of the trough or cut-off low did not exceed 5°W, the peninsular sectors (Murcia and Valencia) of the central Mediterranean coast were the most affected by heavy rainfall. When this axis moved slightly to the east (0°E), then the Balearic Archipelago received the most important rainfall.

Wind direction was decisive in explaining the geographical location of the rainfall peaks in each component. In those affecting the northern sector (Components 1 and 2), the coastal strip was more affected when the winds came from the southeast (Component 1), whereas it rained more in the interior when the winds came from the south (Component 2). The layout of the coastline and the axis of the main relief (Catalan coastal ranges) helped to explain this difference in the distribution of maximum rainfall between the coast and the interior.

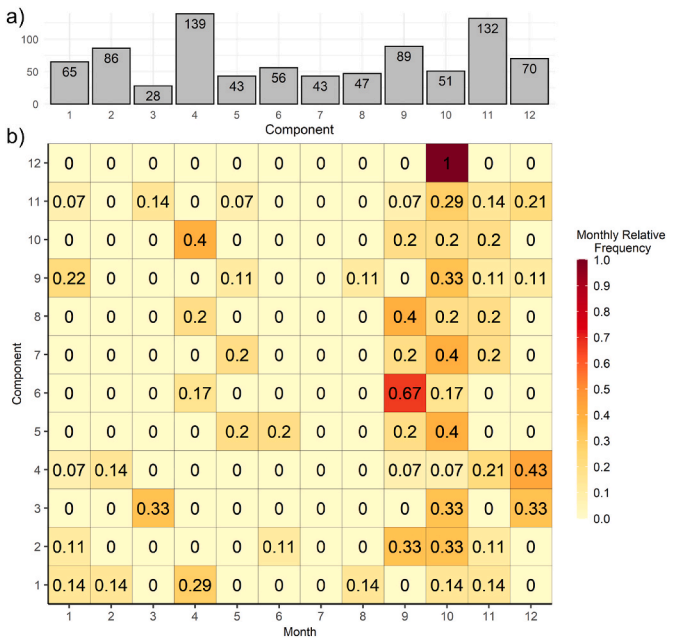

Fig. 6. a) Absolute frequencies, and b) monthly relative frequency for each synoptic situation.

In the central sector, as the wind direction changed direction (S–SE–E–NE), there was a different spatial distribution of the maximum precipitation. The winds from the south provided sufficient humidity for heavy rainfall to develop over the Balearic Islands (Components 9 and 11). For both components, the disposition of the Tramuntana mountain range (SW–NE) explained the location of the maxima in this mountainous area.

In the peninsular part of this central sector, the southeasterly wind was decisive in locating the precipitation peaks in Component 8, being characteristic of the southern part of this central sector (Murcia and Alicante). The maximum daily rainfall was equally distributed across the territories of both provinces (coastal and inland), as the surface wind flow was more from the ESE, therefore having a higher humidity content due to its more-maritime route.

The southeasterly wind was also responsible for the maximum rainfall recorded in the northern part of the central sector of the Mediterranean coast, associated with Components 5 and 12. On the other hand, winds from the east and northeast determined the precipitation peaks recorded in the northern Alicante and southern Valencia (Components 7 and 10). In this case, the disposition of the mountains was also decisive because they converge in the SW–NE (Betic ranges) and NW–SE (Iberian Mountain range) directions, generating a favorable area for the cyclonic rotation of surface winds and the accumulation of large amounts of precipitation. Not unrelated, this was the area of the Mediterranean coast that accumulated the highest maximum precipitation (817 mm in the town of Oliva, on November 4, 1987). With component 10, the rainfall peaks were related to the island of Ibiza, it being close to the coastal strips of southern Valencia and northern Alicante. It should be noted that this central area (Components 6–12) generally exhibited the longest trajectories in the Mediterranean, with some of them (Components 7, 10, and 12) originating in the Gulf of Tunisia. This is the area with the highest sea surface temperatures (SSTs) in the Western Mediterranean, which means greater humidity.

On the other hand, in the southern sector of the Mediterranean coast, Components 3 and 4 coincided with the circulation of surface winds from the southwest or WSW, which drove humidity from the Gulf of Cadiz and the Strait of Gibraltar towards the coasts of Malaga, Granada, and Almeria. In these cases, the disposition of the Betic ranges (SW–NE) explained the coastal location of the precipitation peaks, and the accumulation of more-southerly maxima (Gibraltar and the southern coast of Malaga) when the flows had a more southwesterly component. Component 6, on the other hand, was associated with southeasterly winds, and the rainfall peaks were located along the coast of Almeria, over Granada and northern Malaga province. Also in this case, the disposition of the axis of the Betic ranges favored the maximum coastal rainfall.

Components 4 and 11 are the most frequent (139 and 132 cases, respectively), meanwhile component 3 (28 cases) is less frequent (Fig. 6a). The monthly distributions of these 12 components showed a primary frequency of development, overall, in the fall, and a secondary peak in winter and spring. Only Components 1 and 9 had a certain representativeness in the summer months (Fig. 6b).

4. Discussion and conclusions

In the present study, we were able to identify 899 torrential rainfall events between 1950 and 2020 that exceeded 150 mm in 24 h using 3,537 observational records. Application of the NNMF method allowed us to classify all these events into a determined number of components. Based on the expertise of the research team, 12 different components were identified that represent the geographical distribution of the torrential events very well. Ten of these components describe mainland torrential events, with two characterizing extreme precipitation situations over the Balearic Islands. The trend analysis showed that Components 6–8 experienced a significant increase in accumulated volumes.

The results presented here show that a significant number of the torrential rainfall situations were related to cut-off-low configurations, as determined in the previous work of Muñoz et al. (2020), where it was highlighted that these kinds of situations had an increased frequency of 20% in recent years. Component 1 coincided with the most frequent torrential rainfall events (>100 mm) at the eastern end of the Pyrenees (Lemus-Canovas et al., 2021). Component 2 equated to the findings of Lemus-Canovas et al. (2019) for the eastern Pyrenees. This increasing trend was detected in Components 6 and 8. Insua-Costa et al. (2021) found that the main trajectories of the moisture inputs in the region had tropical and subtropical origins. This was partially detected in the present study, where eastern advections were identified, in addition to the southern ones, thus being in partial agreement with Cloux et al. (2021). Component 7 was also characterized by a high probability of the occurrence of a Saharan dust intrusion (Russo et al., 2020). The trend analysis showed that only seven of the 12 components had positive trends in accumulated rainfall and frequency, which partially concurs with the increasing probability of the occurrence of extreme episodes posited by Myhre et al. (2019). Lorente-Plazas et al. (2020) linked this increase in atmospheric river situations, but this type of configuration was not found in this study.

Components 9 and 11 showed extreme precipitation events over the Balearic Islands that were related to cut-off lows and troughs in the mid-troposphere, in agreement with Grimalt-Gelabert et al. (2021). For the southern Mediterranean coast, the fluxes concurred with the findings of Senciales-González and Ruiz-Sinoga (2021). These components also highlighted northern and northeastern advections, differing from the eastern component detected by Grimalt-Gelabert et al. (2021). Cardoso et al. (2020) pointed out that climate change will likely influence annual precipitation amounts and torrential rainfall events. In this warming context, a rise in SSTs in the Western Mediterranean is expected, increasing moisture inputs under advection trajectories over this area—as detected in the present study—that may lead to an increase in convective precipitation (Llasat et al., 2021). This has also been detected in the eastern part of the Western Mediterranean Basin. This accords with the higher frequency of these events in the autumn months (September–November), when the SSTs in the Mediterranean are at their highest.

The major part of the synoptic configurations is related to unstable situations in the mid-troposphere, with cut-off lows and troughs. In this

kind of configuration, we were also able to identify sea-component advections at slp that brought moist air into the study area. These advections varied from northern to eastern components for the situations occurring over the extreme northernmost part of the study area and the Balearic Islands, to eastern to southeastern components for events occurring along the eastern and southern Mediterranean coasts of the Iberian Peninsula. These fluxes guarantee a trajectory of surface air masses over the Western Mediterranean Sea (with SSTs increasing through the years) before reaching the coast. This indicates moist air coming into contact with the different coastal ranges and being forced to ascend. The sum of these two processes—atmospheric instability and orographic precipitation—led to torrential rainfall events across the study region. As has been pointed out, most of these situations took place in the autumn, especially in September and October, when SSTs are at their most elevated in the Western Mediterranean. Although there are some synoptic patterns with significant IVT, many of the situations depended exclusively on the low altitude and, above all, the direction of the surface flow. It has been noted that the wind direction seems to be a key factor to trigger extreme precipitation events, especially when there is an orographic feature perpendicular to the flow. The areas most affected were those where the surface flow was perpendicular to the coastline or the relevant mountain range, and explains the geographical location of the rainfall peaks in each component. The water vapor transport seems to be a significant factor of the occurrence of extreme precipitation events when the moisture trajectories are originated in the Western Mediterranean, an area with high SSTs, meaning a greater moisture supply. A deeper analysis is needed to evaluate longer trajectories through high SSTs areas, as well as the role played by atmospheric rivers (Ramos et al., 2015; Lorente-Plazas et al., 2020; Hénin et al., 2021).

Authorship statement

Juan Javier Miró: Data curation, Methodology, Investigation. Marc Lemus-Cánovas: Methodology, Visualization. Javier Martin-Vide: Formal analysis, Supervision. Roberto Serrano-Notivoli: Data curation. Jorge Olcina Cantos: Conceptualization, Formal analysis, Writing-original draft. María J. Estrela: Formal analysis. Pablo Sarricolea: Validation. Oliver Meseguer-Ruiz: Conceptualization, Funding acquisition, Formal analysis, Writing-original draft.

Declaration of competing interest

The authors declare that they have no known competing financial interests or personal relationships that could have appeared to influence the work reported in this paper.

Acknowledgements

The authors want to thank the Proyecto UTA-Mayor N° 5807–22 from the Universidad de Tarapacá, Chile. MLC, JMV, PS and OMR want to thank the Climatology Group (2017SGR1362, Catalan Government). RSN is partially supported by the Universidad Autónoma de Madrid (UAM) and the Comunidad de Madrid through project SI3-PJI-2021-00398, the Natural Hazards and Global Change research group from UAM, and the Government of Aragón through the "Program of research groups" (group H09_20R, "Climate, Water, Global Change, and Natural Systems"). JJM and MJE participation has been funded by the Spanish Ministerio de Ciencia e Innovación through the research project PID2020-118797RB-I00 (MCIN/AEI/10.13039/501100011033) and by Generalitat Valenciana through the research project PROMETEO/2021/016 (Conselleria d'Innovació, Universitats, Ciència i Societat Digital).

References

Blackport, R., Screen, J.A., 2020. Insignificant effect of Arctic amplification on the amplitude of midlatitude atmospheric waves. Sci. Adv. 6, eaay2880 https://doi.org/10.1126/sciadv.aay2880.

Cardoso, S., Martinho, M.A., Carvalho, A.C., Rocha, A., 2020. Extreme precipitation events under climate change in the Iberian Peninsula. Int. J. Climatol. 40, 1255–1278. https://doi.org/10.1002/joc.6269.

Casanueva, A., Rodriguez-Puebla, C., Frias, M.D., Gonzalez-Reviriego, N., 2014. Variability of extreme precipitation over Europe and its relationships with teleconnection patterns. Hydrol. Earth Syst. Sci. 18, 709–725. https://doi.org/10.5194/hess-18-709-2014.

CEDEX, 2021. Impacto del cambio climático en las precipitaciones máximas en España. Centro de Estudios Hidrográficos, Gobierno de España, Madrid, p. 404.

Cipolla, G., Francipane, A., Noto, L.V., 2020. Classification of extreme rainfall for a Mediterranean region by means of atmospheric circulation patterns and reanalysis data. Water Resour. Manag. 34, 3219–3235. https://doi.org/10.1007/s11269-020-02609-1.

Cloux, S., Garaboa-Paz, D., Insua-Costa, D., Miguez-Macho, G., Pérez-Muñuzuri, V., 2021. Extreme precipitation events in the Mediterranean area: contrasting two different models for moisture source identification. Hydrol. Earth Syst. Sci. 25, 6465–6477. https://doi.org/10.5194/hess-25-6465-2021.

Cramer, W., Guiot, J., Fader, M., Garrabou, J., Gattuso, J.P., Iglesias, A., Lange, M.A., Lionello, P., Llasat, M.C., Paz, S., Penuelas, J., Snoussi, M., Toreti, A., Tsimplis, M.N., Xoplaki, E., 2018. Climate change and interconnected risks to sustainable development in the Mediterranean. Nat. Clim. Change 8, 972–980. https://doi.org/10.1038/s41558-018-0299-2.

Davolio, S., Della Fera, S., Laviola, S., Miglietta, M.M., Levizzani, V., 2020. Heavy precipitation over Italy from the Mediterranean storm "Vaia" in October 2018: assessing the role of an atmospheric river. Mon. Weather Rev. 148, 3571–3588. https://doi.org/10.1175/MWR-D-20-0021.1.

del Rio, S., Herrero, L., Fraile, R., Penas, A.P., 2011. Spatial distribution of recent rainfall trends in Spain (1961–2006). Int. J. Climatol. 31, 656–667. https://doi.org/10.1002/joc.2111.

Ferreira, R.N., 2021. Cut-off low and extreme precipitation in eastern Spain: current and future climate. Atmosphere 12 (7), 835. https://doi.org/10.3390/atmos12070835.

Francis, F.A., Vavrus, S.J., 2012. Evidence linking Arctic amplification to extreme weather in mid-latitudes. Geophys. Res. Lett. 39, L06801 https://doi.org/10.1029/2012GL051000.

Gil-Guirado, S., Pérez-Morales, A., Pino, D., Peña, J.C., López Martínez, F., 2022. Flood impact on the Spanish Mediterranean coast since 1960 based on the prevailing synoptic patterns. Sci. Total Environ. 807, 150777 https://doi.org/10.1016/j.scitotenv.2021.150777.

Grimalt-Gelabert, M., Alomar-Garau, G., Martin-Vide, J., 2021. Synoptic causes of torrential rainfall in the Balearic islands (1941–2010). Atmosphere 12 (8), 1035. https://doi.org/10.3390/atmos12081035.

Halifa-Marín, A., Lorente-Plazas, R., Pravia-Sarabia, E., Montávez, J.P., Jiménez-Guerrero, P., 2021. Atlantic and Mediterranean influence promoting an abrupt change in winter precipitation over the southern Iberian Peninsula. Atmos. Res. 253, 105485 https://doi.org/10.1016/j.atmosres.2021.105485.

Hénin, R., Ramos, A.M., Pinto, J.G., Liberato, M.L.R., 2021. A ranking of concurrent precipitation and wind events for the Iberian Peninsula. Int. J. Climatol. 41, 1421–1437. https://doi.org/10.1002/joc.6829.

Hersbach, H., Bell, B., Berrisford, P., Hirahara, S., Horányi, A., Muñoz-Sabater, J., Nicolas, J., Peubey, C., Radu, R., Schepers, D., Simmons, A., Soci, C., Abdalla, S., Abellan, X., Balsamo, G., Bechtold, P., Biavati, G., Bidlot, J., Bonavita, M., De Chiara, G., Dahlgren, P., Dee, D., Diamantakis, M., Dragani, R., Flemming, J., Forbes, R., Fuentes, M., Geer, A., Haimberger, L., Healy, S., Hogan, R.J., Hólm, E., Janiskova, M., Keeley, S., Laloyaux, P., Lopez, P., Lupu, C., Radnoti, G., de Rosnay, P., Rozum, I., Vamborg, F., Villaume, S., Thépaut, J.N., 2020. The ERA5 global reanalysis. Q. J. R. Meteorol. Soc. 146, 1999–2049. https://doi.org/10.1002/qj.3803.

Insua-Costa, D., Miguez-Macho, G., Llasat, M.C., 2019. Local and remote moisture sources for extreme precipitation: a study of the two catastrophic 1982 western Mediterranean episodes. Hydrol. Earth Syst. Sci. 23, 3885–3900. https://doi.org/10.5194/hess-23-3885-2019.

Insua-Costa, D., Lemus-Cánovas, M., Miguez-Macho, G., Llasat, M.C., 2021. Climatology and ranking of hazardous precipitation events in the western Mediterranean area. Atmos. Res. 255, 105521 https://doi.org/10.1016/j.atmosres.2021.105521.

IPCC, 2021. In: Masson-Delmotte, V., Zhai, P., Pirani, A., Connors, S.L., Péan, C., Berger, S., Caud, N., Chen, Y., Goldfarb, L., Gomis, M.I., Huang, M., Leitzell, K., Lonnoy, E., Matthews, J.B.R., Maycock, T.K., Waterfield, T., Yelekçi, O., Yu, R., Zhou, B. (Eds.), Climate Change 2021: the Physical Science Basis. Contribution of Working Group I to the Sixth Assessment Report of the Intergovernmental Panel on Climate Change. Cambridge University Press. In Press.

Kendall, M.G., 1962. Rank Correlation Methods. Hafner Publishing Company, New York.

Kim, G.U., Seo, K.H., Chen, D., 2019. Climate change over the Mediterranean and current destruction of marine ecosystem. Sci. Rep. 9, 18813 https://doi.org/10.1038/s41598-019-55303-7.

Krichak, S.O., Barkan, J., Breitgand, J.S., Gualdi, S., Feldstein, S.B., 2015. The role of the export of tropical moisture into midlatitudes for extreme precipitation events in the Mediterranean region. Theor. Appl. Climatol. 121, 499–515. https://doi.org/10.1007/s00704-014-1244-6.

Lavers, D.A., Allan, R.P., Wood, E.F., Villarini, G., Brayshaw, D.J., Wade, A.J., 2011. Winter floods in Britain are connected to atmospheric rivers. Geophys. Res. Lett. 38, L23803 https://doi.org/10.1029/2011GL049783.

Lavers, D.A., Villarini, G., 2015. The contribution of atmospheric rivers to precipitation in Europe and the United States. J. Hydrol. 522, 382–390. https://doi.org/10.1016/j.jhydrol.2014.12.010.

Lavers, D.A., Villarini, G., Allan, R.P., Wood, E.F., Wade, A.J., 2012. The detection of atmospheric rivers in atmospheric reanalyses and their links to British winter floods and the large-scale climatic circulation. J. Geophys. Res. Atmos. 117, D20106 https://doi.org/10.1029/2012JD018027.

Lemus-Canovas, M., Ninyerola, M., Lopez-Bustins, J.A., Manguan, S., Garcia-Sellés, C., 2019. A mixed application of an objective synoptic classification and spatial regression models for deriving winter precipitation regimes in the Eastern Pyrenees. Int. J. Climatol. 39 (4), 2244–2259. https://doi.org/10.1002/joc.5948.

Lemus-Canovas, M., Lopez-Bustins, J.A., Martín-Vide, J., Halifa-Marin, A., Insua-Costa, D., Martinez-Artigas, J., Trapero, L., Serrano-Notivoli, R., Cuadrat, J.M., 2021. Characterisation of extreme precipitation events in the Pyrenees: from the local to the synoptic scale. Atmosphere 12, 665. https://doi.org/10.3390/atmos12060665.

Llasat, M.C., del Moral, A., Cortès, M., Rigo, T., 2021. Convective precipitation trends in the Spanish Mediterranean region. Atmos. Res. 257, 105581 https://doi.org/10.1016/j.atmosres.2021.105581.

Lopez-Bustins, J.A., Lemus-Canovas, M., 2021. The influence of the western Mediterranean oscillation upon the spatio-temporal variability of precipitation over Catalonia (northeastern of the Iberian Peninsula). Atmos. Res. 236, 104819 https://doi.org/10.1016/j.atmosres.2019.104819.

Lorente-Plazas, R., Montavez, J.P., Ramos, A.M., Jerez, S., Trigo, R.M., Jimenez-Guerrero, P., 2020. Unusual atmospheric-river-like structures coming from Africa induce extreme precipitation over the western Mediterranean Sea. J. Geophys. Res. Atmos. 125, e2019JD031280 https://doi.org/10.1029/2019JD031280.

Li, Y., Ngom, A., 2013. The non-negative matrix factorization toolbox for biological data mining. Source Code Biol. Med. 8, 10. https://doi.org/10.1186/1751-0473-8-10.

Mann, H.B., 1945. Nonparametric tests against trend. Econometrica 13, 245–259. https://doi.org/10.2307/1907187.

Mastrantonas, N., Herrera-Lormendez, P., Magnusson, L., Pappenberger, F., Matschullat, J., 2021. Extreme precipitation events in the Mediterranean: spatiotemporal characteristics and connection to large-scale atmospheric flow patterns. Int. J. Climatol. 41, 2710–2728. https://doi.org/10.1002/joc.6985.

Michaelides, S., Karacostas, T., Sánchez, J.L., Retalis, A., Pytharoulis, I., Homar, V., Romero, R., Zanis, P., Giannakopoulos, C., Buhl, J., Ansmann, A., Merino, A., Melcón, P., Lagouvardos, K., Kotroni, V., Bruggeman, A., López-Moreno, J.I., Berthet, C., Katragkou, E., Tymviosa, F., Hadjimitsis, D.G., Mamouri, R.E., Nisantzi, A., 2018. Reviews and perspectives of high impact atmospheric processes in the Mediterranean. Atmos. Res. 208, 4–44. https://doi.org/10.1016/j.atmosres.2017.11.022.

Merino, A., Fernández-Vaquero, M., López, L., Fernández-González, S., Hermida, L., Sánchez, J.L., García-Ortega, E., Gascón, E., 2016. Large-scale patterns of daily precipitation extremes on the Iberian Peninsula. Int. J. Climatol. 36, 3873–3891. https://doi.org/10.1002/joc.4601.

Meseguer-Ruiz, O., Osborn, T.J., Sarricolea, P., Jones, P.D., Olcina Cantos, J., Serrano-Notivoli, R., Martin-Vide, J., 2019. Definition of a temporal distribution index for high temporal resolution precipitation data over peninsular Spain and the Balearic Islands: the fractal dimension; and its synoptic implications. Clim. Dynam. 52, 439–456. https://doi.org/10.1007/s00382-018-4159-6.

Meseguer-Ruiz, O., Lopez-Bustins, J.A., Arbiol-Roca, L., Martin-Vide, J., Miro, J., Estrela, M.J., 2021. Temporal changes in extreme precipitation and exposure of tourism in Eastern and South-Eastern Spain. Theor. Appl. Climatol. 144, 379–390. https://doi.org/10.1007/s00704-021-03548-6.

Miro, J.J., Caselles, V., Estrela, M.J., 2017. Multiple imputation of rainfall missing data in the Iberian Mediterranean context. Atmos. Res. 197, 313–330. https://doi.org/10.1016/j.atmosres.2017.07.016.

Miro, J.J., Estrela, M.J., Caselles, V., Gómez, I., 2018. Spatial and temporal rainfall changes in the Júcar and Segura basins (1955-2016): finescale trends. Int. J. Climatol. 38, 4699–4722. https://doi.org/10.1002/joc.5689.

Miro, J.J., Estrela, M.J., Olcina-Cantos, J., Martin-Vide, J., 2021. Future projection of precipitation changes in the Júcar and Segura river basins (Iberian Peninsula) by CMIP5 GCMs local downscaling. Atmosphere 12, 879. https://doi.org/10.3390/atmos12070879.

Moline, G., Deque, M., Coppola, E., Blanchet, J., Neppel, L., 2016. Heavy precipitation in the Mediterranean basin. In: Moatti, J.P., Thiébault, S. (Eds.), The Mediterranean Region under Climate Change. IRD Éditions, Marseille, pp. 107–114. https://doi.org/10.4000/books.irdeditions.22908.

Muñoz, C., Schultz, D., Vaughan, G., 2020. A midlatitude Climatology and interannual variability of 200- and 500-hPa cut-off lows. J. Clim. 33 (6), 2201–2222. https://doi.org/10.1175/JCLI-D-19-0497.1.

Myhre, G., Alterskjær, K., Stjern, C.W., Hodnebrog, o, Marelle, L., Samset, B.H., Sillmann, J., Schaller, N., Fischer, E., Schulz, M., Stohl, A., 2019. Frequency of extreme precipitation increases extensively with event rareness under global warming. Sci. Rep. 9, 16063 https://doi.org/10.1038/s41598-019-52277-4.

Olcina Cantos, J., Serrano-Notivoli, R., Miro, J., Meseguer-Ruiz, O., 2019. Tropical nights on the Spanish Mediterranean coast, 1950−2014. Clim. Res. 78, 225–236. https://doi.org/10.3354/cr01569.

Osso, A., Allan, R.P., Hawkins, E., Shaffrey, L., Maraun, D., 2021. Emerging new climate extremes over Europe. Clim. Dynam. https://doi.org/10.1007/s00382-021-05917-3.

Ramos, A.M., Trigo, R.M., Liberato, M.L.R., Tome, R., 2015. Daily precipitation extreme events in the Iberian Peninsula and its association with atmospheric rivers. J. Hydrometeorol. 16 (2), 579–597. https://doi.org/10.1175/JHM-D-14-0103.1.

Ramos, A.M., Trigo, R.M., Tomé, R., Liberato, M.L.R., 2018. Impacts of atmospheric rivers in extreme precipitation on the European Macaronesian islands. Atmosphere 9, 325. https://doi.org/10.3390/atmos9080325.

Russo, A., Sousa, P.M., Durão, R.M., Ramos, A.M., Salvador, P., Linares, C., Díaz, J., Trigo, R.M., 2020. Saharan dust intrusions in the Iberian Peninsula: predominant synoptic conditions. Sci. Total Environ. 717, 137041 https://doi.org/10.1016/j.scitotenv.2020.137041.

Sen, P.K., 1968. Estimates of the regression coefficient based on Kendall's tau. J. Am. Stat. Assoc. 63, 1379–1389.

Senciales-González, J.M., Ruiz-Sinoga, J.D., 2021. Features of weather types involving heavy rainfall along the Southern Spanish Mediterranean. Cuadernos de Investigación Geográfica 47, 221–242. https://doi.org/10.18172/cig.4765.

Serrano-Notivoli, R., De Luis, M., Beguería, S., 2017a. An R package for daily precipitation climate series reconstruction. Environ. Model. Software 89, 190–195. https://doi.org/10.1016/j.envsoft.2016.11.005.

Serrano-Notivoli, R., Beguería, S., Saz, M.A., Longares, L.A., de Luis, M., 2017b. SPREAD: a high-resolution daily gridded precipitation dataset for Spain – an extreme events frequency and intensity overview. Earth Syst. Sci. Data 9, 721–738. https://doi.org/10.5194/essd-9-721-2017.

Serrano-Notivoli, R., Beguería, S., Saz, M.A., de Luis, M., 2018. Recent trends reveal decreasing intensity of daily precipitation in Spain. Int. J. Climatol. 38, 4211–4224. https://doi.org/10.1002/joc.5562.

Sra, S., Dhillon, I.S., 2006. Generalized nonnegative matrix approximations with Bregman divergences. Adv. Neural Inf. Process. Syst. 18. Adv. Neural Inf. Process. Syst. https://dl.acm.org/doi/10.5555/2976248.2976284.

Tapiador, F.J., Marcos, C., Sancho, J.M., Santos, C., Núñez, J.A., Navarro, A., Kummerow, C., Adler, R.F., 2021. The September 2019 floods in Spain: an example of the utility of satellite data for the analysis of extreme hydrometeorological events. Atmos. Res. 257, 105588 https://doi.org/10.1016/j.atmosres.2021.105588.

Tandon, R., Sra, S., 2010. Sparse Nonnegative Matrix Approximation: New Formulations and Algorithms. Max Planck Institute for Biological Cybernetics. Technical Report No. 193.

Zittis, G., Bruggeman, A., Lelieveld, J., 2021. Revisiting future extreme precipitation trends in the Mediterranean. Weather Clim. Extrem. 34, 100380 https://doi.org/10.1016/j.wace.2021.100380.